Nanoscale

Simulations of the effect of an oxide on contact area measurements from conductive atomic force microscopy

Journal:	*Nanoscale*
Manuscript ID	NR-ART-10-2018-008605.R1
Article Type:	Paper
Date Submitted by the Author:	07-Dec-2018

Complete List of Authors:	Chen, Rimei; University of California Merced School of Engineering Vishnubhotla, Sai Bharadwaj; University of Pittsburgh, Mechanical Engineering and Materials Science Jacobs, Tevis; University of Pittsburgh, Mechanical Engineering & Materials Science Martini, Ashlie; University of California Merced,

Simulations of the effect of an oxide on contact area measurements from conductive atomic force microscopy

Rimei Chen[1], Sai Bharadwaj Vishnubhotla[2], Tevis D. B. Jacobs[2], Ashlie Martini[1*]

1. Department of Mechanical Engineering, University of California-Merced, Merced, CA, 95301, USA.
2. Department of Mechanical Engineering and Materials Science, University of Pittsburgh, Pittsburgh, PA, 15213, USA.

* Corresponding author: amartini@ucmerced.edu

Abstract

Nanoscale contact area in conductive atomic force microscopy can be determined by analyzing current flow using electron transport theories. However, it is recognized that native oxides on the conductive tip will reduce current flow, thus degrading the accuracy of the measured contact area. To quantify the adverse effect of an oxide on contact area measurements, we use molecular dynamics simulations of an oxide-coated platinum tip and a crystalline platinum substrate, where both the contact size and conductance can be inferred from the positions of atoms in the interface. We develop a method to approximate conductance based on the distance between atoms in platinum channels across the contact. Then, we compare the contact area calculated from conductance with ballistic transport and tunneling theories to that obtained using the known positions of atoms in the contact. The difference is small for very thin (<0.1 nm) or thick (>1.0 nm) oxides, where ballistic transport and tunneling theories work well; however, the difference can be significant for oxides between these limits, which is expected to be the case for platinum in many practical applications.

I. INTRODUCTION

Understanding and predicting contact area at the nanoscale is important for probe-based microscopy,[1,2] nanolithography,[3] and nanodevices.[4–6] For example, in scanning probe microscopy, the resolution of topography and properties measurements depends on the contact size.[7] For nanoscale electromechanical switches, the size of the contact between the source and gate controls the current flow and therefore determines the performance of these devices.[5]

Since the contact is buried in the interface between two bodies, it is difficult to directly measure contact area using experimental techniques. However, conductive atomic force microscopy (c-AFM) has enabled the indirect measurement of contact area through the electrical contact conductance. In c-AFM, a bias voltage V is applied between the tip and substrate, the resultant current I is measured, and the electrical conductance G is determined from slope of the I-V curve. Then, under the assumption that contact radius a is smaller than the mean free path of an electron l_f, it is common to relate conductance and contact area using the Sharvin equation for ballistic transport:

$$G_s = 3A_S/4\rho l_f \quad (1)$$

where ρ is resistivity and A_S is contact area. The proportionality of conductance and contact area has been shown to be accurate for nanometer-scale contacts,[8–10] and even for metallic junctions thinned down to single-atom width.[11,12] However, the Sharvin equation does not account for the presence of insulating layers on the contacting surfaces. Such insulating layers, including oxides, adsorbates, or contaminants, are common on surfaces in real-world applications and under most experimental conditions.[13,14] The presence of insulating layers can prevent the formation of metallic contact, and prior work by the present authors suggests that, in such cases, electron transport theories can overpredict current flow across a platinum nanocontact by a factor of 20.[15] This overprediction is due to the fact that, with an insulating film, conduction only occurs by tunneling across the interface. In this case, the relationship between conductance and contact area A_T is described by tunneling theory:[15,16]

$$G_T = \left(3.16 \times 10^{14} \sqrt{\phi} \frac{1}{t} \exp\left(-1.025 t \sqrt{\phi}\right)\right) A_T \quad (2)$$

where ϕ is the mean barrier height and t is the oxide thickness. This tunneling model has been used to calculate contact area from c-AFM measurements with an oxide-containing conductive platinum tip.[15,17]

Therefore, previous research suggests that ballistic transport theories can be used to calculate contact area from conductance if no insulating layer is present and tunneling theories apply for a thick insulating layer. However, many real contacts may exist between these limiting cases. For example, Pt is relevant for many applications that rely on nanoscale contacts [18–20] and Pt surfaces may have a native oxide layer that is less than 0.5 nm.[15,21] The accuracy of ballistic transport or tunneling theories for calculating contact area in these cases is unknown because area and conduction cannot be measured independently. Furthermore, a common approach in experimental studies is to simply use c-AFM with the Sharvin equation, regardless of the possible presence of thin insulating layers.[8,22,23]

Atomistic simulations can provide some insight into the effect of insulating layers because they explicitly model the size and morphology of the contact. Density functional theory or *ab initio* molecular dynamics enable the direct calculation of conduction,[24–28] but are limited to very small size scales and so cannot capture the deformation at technologically relevant size scales. Alternatively, classical molecular dynamics (MD) simulations can model nanoscale contacts accurately,[15,29] but do not include electrons and so cannot directly calculate conduction. There have been extensions of classical MD developed that enable calculation of conduction,[30,31] but the approach does not differentiate between atom types and so cannot be used to investigate the effect of insulating layers. Finally, a recent study by Yang, *et al.*[29] used classical MD simulations to understand the effect of small amounts of adsorbates on conduction in Pt nanoasperities for nanoelectromechanical switches. The authors showed that adsorbates can partially or completely block metal-metal contact, and described a balance where some adsorbates are advantageous for minimizing plastic deformation, but too many adsorbates will block the current flow. However, this study considered current flow through direct metal-metal contact and did not attempt to include contributions due to tunneling, which may play a significant role in the case where one or more of the metals has at least a monolayer of oxide coverage.

In the present study, we used MD simulations to model the nanoscale contact between a platinum tip with an oxide and a pristine platinum substrate, where conductance was approximated using an empirical model that included both direct metallic and tunneling conduction. The goal was to evaluate the accuracy of contact area measurements obtained using conventional experimental c-AFM techniques with ballistic transport theories in cases where a thin oxide layer is present. The approach consisted of five steps: (1) Identify channels of platinum atoms across the interface; (2) approximate the total conductance based on an empirical model relating conductance to atom distance in the channels; (3) calculate the contact area from the conductance using ballistic transport and tunneling theories; (4) calculate the *true* contact area using positions of atoms in the contact; and (5) determine the difference between contact area calculated from conductance and that from atom positions as a function of oxide thickness. The contact area calculated from conductance is comparable to the approach used in a typical c-AFM experiment, so the difference between this value and the area obtained from atomic positions reflects the underestimation that might be expected in an experiment.

II. METHODS

Figure 1(a) shows a snapshot of a model oxide-coated platinum tip and atomically flat platinum substrate. The Pt tip was parabolic with a radius of 2 nm and a height of 5 nm. The tip radius and height were chosen to be big enough to minimize the effects of boundaries on the contact stress distribution.[32] The crystalline region of the tip had a crystallographic orientation of [1 -42 31] in the z-direction. This orientation was randomly chosen but was selected to ensure a rounded tip apex could be achieved for this small tip size. The dimensions of the flat Pt substrate were 9.0 × 8.8 × 3.0 nm^3 in x-, y-, and z-directions, respectively, with a crystallographic orientation of [1 1 1] in the z-direction. Periodic boundary conditions were applied along the x- and y-directions and the boundary was fixed in the z-direction.

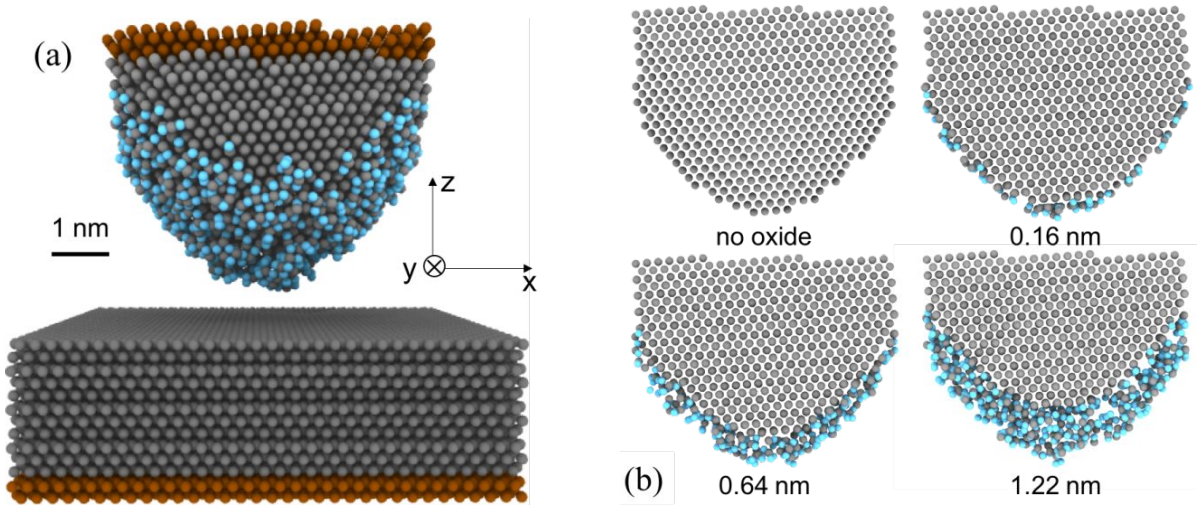

Figure 1: (a) Snapshot of the model of an oxide-coated Pt tip and a flat Pt substrate; (b) Cross-sections of the Pt tips with varying oxide thickness: 0 nm (no oxide), 0.16 nm (approximately one monolayer), 0.64 nm, and 1.22 nm. The outermost radius of all model tips is 2 nm. The grey color represents platinum atoms, the blue color represents oxygen atoms and the brown color represents rigid platinum atoms.

The topmost 0.5 nm of the tip and the bottommost 0.5 nm of the substrate were treated as rigid bodies. A Nosé-Hoover thermostat was applied to the 2-nm region adjacent to the rigid layers in both tip and substrate to maintain the temperature of the system at 300 K. The remainder of the tip and the substrate were integrated using the NVE (constant number of atoms, volume, and energy) ensemble, which ensured interactions of the atoms between the tip and the substrate without a significant effect of the thermostat.[33] All interatomic interactions were modeled using the ReaxFF potential[34] with a time step of 0.25 fs. This potential was previously shown to predict the bulk properties of Pt, as well as oxygen adsorption and oxide formation on Pt surfaces, in reasonable agreement with both density functional theory calculations and experiment observations.[34,35] Simulations were carried out using the large-scale atomic/molecular massively parallel simulator (LAMMPS).[36]

Seven model tips were created by combining a crystalline Pt core with amorphous Pt oxide shells of varying thickness. First, a periodic box containing amorphous platinum dioxide was created by heating α-PtO_2 to 2000 K and then quenching to room temperature. α-PtO_2 was used because the surface oxide for platinum usually has a Pt-to-O ratio of 1:2.[21,37] Then, a thin shell of oxide was cut from the box where the inner radius of the shell was the same as the outer radius of the crystalline Pt core. Simulations were run at 500 K until the potential energy reached steady state, which required an average of 7 ps. After the oxidized Pt tips equilibrated, the thickness of the oxide layer was re-characterized by calculating the average distance between the crystalline profile and the oxide profile at 40 positions on a cross-section of the tip. Seven Pt tips were created with varying oxide thickness: t=0 nm (no oxide), 0.16 nm (approximately one monolayer), 0.40 nm, 0.64 nm, 1.00 nm, 1.15 nm, and 1.22 nm; four of these are shown in Fig. 1(b).

Each Pt tip was initially placed such that the center of the bottommost atom of the tip was 1 nm above the center of the topmost atom of the substrate. This distance is larger than the cutoff distance of the potential which ensured that there was no interaction between the tip and the substrate at the start of the simulation. The tip was then brought into contact with the surface at a speed of 10 m/s. During this process, the penetration of the tip into the substrate δ was calculated as the instantaneous distance between the center of the atoms in the rigid layers subtracted from the sum of the initial heights of the tip and substrate. This calculation of penetration depth is consistent with the definition used in typical contact mechanics models,[38] where zero corresponds to the point at which the tip and substrate would first come into contact if they were rigid bodies. At various times, the tip movement was stopped and the model was relaxed for 50 ps to ensure stable energy and force.[39]

III. RESULTS AND DISCUSSION

To approximate the conductance of the contact between the Pt tip and substrate, we assumed conduction occurred through “channels” of Pt atoms that spanned from the substrate to the crystalline region of the tip. Figure 2(a) shows a representative conduction channel for the model with the 1.15-nm oxide. To identify a conduction channel for a given substrate atom (atom 1 in Fig. 2(a)), we first found the nearest Pt atom (atom 2) in the tip. Then we searched for the next Pt atom (atom 3) which was closest to atom 2 in the tip. This process continued until the next Pt

atom (atom 7) was within the crystalline region of the tip. After identifying a metallic chain, we searched for O atoms between Pt atoms in each chain based on the following criteria: the vertical position of the O atom is between those of two Pt atoms, and the distance between the O atom and each Pt atom is smaller than the distance between the two Pt atoms. Figure 2(a) shows an O atom identified between Pt atom 5 and Pt atom 6. This process was repeated for every atom on the surface of the substrate. Once all possible channels were identified, we approximated conduction as described below.

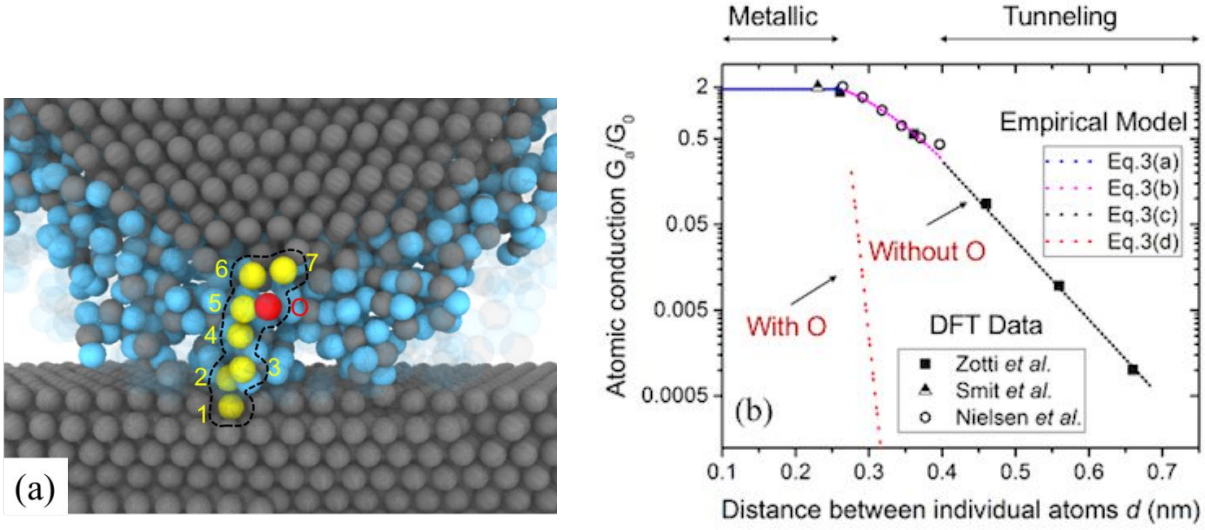

Figure 2: (a) A representative conduction channel (Pt in yellow) was identified with an oxygen atom (red) present for the contact model with the 1.15-nm oxide. (b) Conductance was plotted as a function of distance d between individual atoms. The original data were taken from Ref. [28] (solid squares), Ref. [40] (half-solid triangles), and Ref. [25] (hollow circles). Conductance is approximated using an empirical model (dotted lines) that includes both metallic and tunneling conduction, where the blue, pink, and black lines show the fitted empirical model without oxygen present, and the red line represents the empirical model with oxygen.

Conduction along an atomic channel can occur through two mechanisms, direct metallic contact conduction or tunneling, depending on the distance between atoms. Direct metallic conduction occurs when atoms are close enough for electron transport to occur by ballistic or diffusive mechanisms.[11] The direct metallic conductance of a single Pt atom chain has been found to be 1.5~2.5 G_0,[25,40–43] where G_0 is the quantum conductance ($G_0 = 2e^2/h$). As the distance between atoms increases, the conduction shifts from metallic conduction to tunneling conduction.[16] Previous density functional theory (DFT) calculations have shown that conduction between atoms decays exponentially as their distance increases.[25–28]

Here, we used DFT data from Refs. [25,28,40] to develop an empirical model (Eq. 3) for atom-atom conductance G_a as a function of atom center distance d that captures both the constant conductance of direct metallic conduction and the distance-dependent conductance of tunneling conduction. For atom-atom distances less than 0.27 nm, the conductance was taken to be $1.89G_0$, the average of values reported from previous DFT calculations for direct metallic conductance.[25,28,40] For distances larger than 0.27 nm, two exponential decay functions were used, chosen to fit the available DFT data,[25,28] where the decay rate was larger for distances

greater than 0.4 nm when conduction occurs via pure tunneling. Further, studies have shown that the conduction in silver and copper atom chains decreases if oxygen is present.[44,45] This effect has also been shown for platinum with a hydrogen molecule or carbon and oxide atoms embedded in the chain.[43,46,47] Unfortunately, no previous data is available for platinum chains with oxygen. Therefore, we developed an approximate function based on the expectations that (i) the conductance will decay more quickly with oxygen than without, and (ii) for the thickest oxide (1.22 nm) the total conductance should be consistent with the prediction of classical tunneling theory (Eq. 2). The complete set of equations used to estimate conductance based on atom distance is the following:

$$\frac{G_a}{G_0} = \begin{cases} 1.89, & for\ d \le 0.27\ nm & (3a) \\ e^{(1.46d - 0.43d^2 - 0.24)}, & for\ 0.27 < d \le 0.4\ nm\ and\ without\ O & (3b) \\ e^{(-2.13d + 7.21)}, & for\ d > 0.4\ nm\ and\ without\ O & (3c) \\ e^{(-23.00d + 61.47)}, & for\ d > 0.27\ nm\ and\ with\ O & (3d) \end{cases}$$

The available DFT data and empirical approximations are shown in Fig. 2(b). We note that these equations are approximations based on previous DFT data and limiting behavior predicted by classical tunneling theory, so they are not expected to provide accurate quantitative predictions of conductance.

Eq. 3 was used to calculate the conductance for all atom-atom pairs. The conductance for each channel $G_{channel}$ was then taken as the minimum conductance for atom-atom pairs G_a in that channel, based on the assumption that ballistic transport though an atomic-sized ballistic contact is independent of length.[11] Then, the total conduction for the system G was calculated as the sum of the conductance of all channels acting as resistors in parallel, i.e. $G=G_{channel,1}+G_{channel,2}+\ldots+G_{channel,N}$. The total conductance was calculated using this approach for all model tips as they were brought into contact with the substrate.

Figure 3 shows the conductance as a function of time for six different oxide thickness models at a penetration depth of $\delta = 0.06$ nm. At 0 ns, the tip started moving toward the substrate. Then, at 0.073 ns, the downward motion was stopped and the tip was held in place until the system equilibrated. In all cases, the conductance increased during loading and then fluctuated about a constant value during equilibration. Tips with thicker oxide layers exhibited a slower increase in conductance with time and a smaller steady state value.

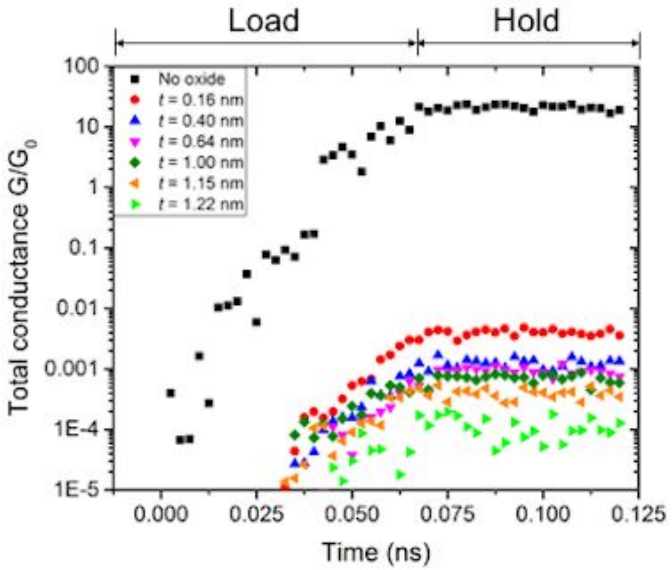

Figure 3: The total conductance as a function of time calculated for six different oxide thicknesses. The tips were brought to the same vertical position (δ = 0.06 nm) and held at that position to allow equilibration.

Figure 4(a) shows the conductance as a function of oxide thickness at three penetration depths: δ = 0.06 nm, 0.14 nm, and 0.19 nm, which correspond to average normal loads of -3 nN, 28 nN, and 37 nN, respectively, for the no-oxide tip. The error bars on the conductance reflect the standard deviation of the data during the relaxation period. The position and shape of the tip relative to the substrate at each depth are illustrated in Fig. 4(b). In general, the conductance is larger as the tip moves further into the substrate. This is due to both an increase in contact size and a decrease in the distance between atoms in the conduction channels. Also, at all depths, the conductance decays rapidly with increasing oxide thickness, consistent with observations from experimental studies of insulating films between metal-metal junctions.[18,41,48]

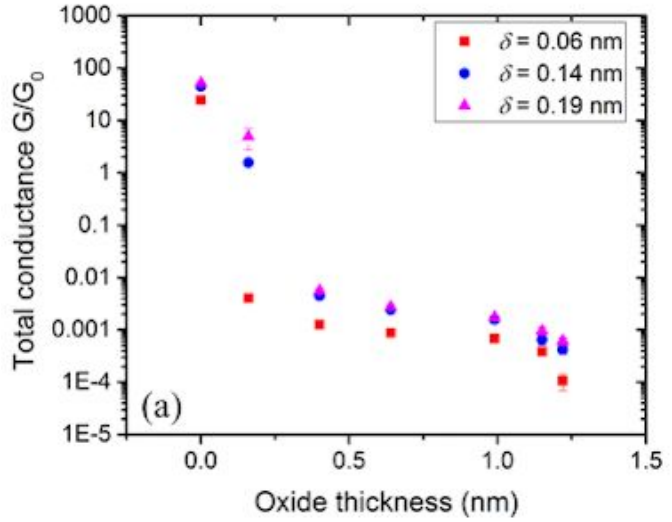

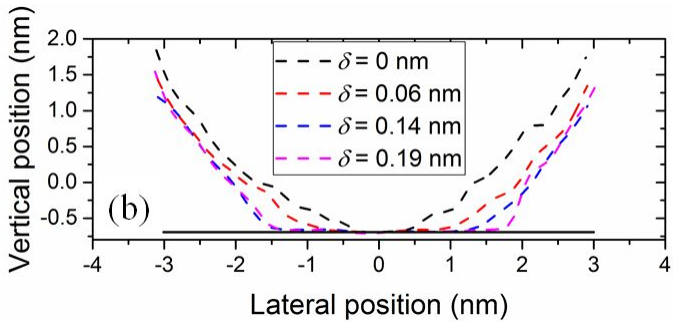

Figure 4: (a) The conductance as a function of oxide thickness for various penetration depths. The error bars represent the standard deviation during the relaxation period. (b) Profiles of the tip at different penetration depths. The dashed lines are the profiles of the tip and the black solid line is the original position of the substrate. These profiles are from the tip without an oxide but are representative of the other cases.

To mimic a typical c-AFM experiment, the conductance (which is determined as described above) was used to calculate a computed contact area using equations for both ballistic transport and tunneling theory. First, the Sharvin equation (Eq. 1) was used to calculate contact area A_s, where bulk platinum values[15] were used for the resistivity (ρ = 10.6 $\mu\Omega$ cm) and mean free path (l_f = 7 nm). Second, tunneling theory (Eq. 2) was used to calculate contact area A_T, where the mean barrier height was ϕ = 0.31 eV (reported previously for contact between an oxidized Pt tip and a Pt surface[49]) and the oxide thickness was measured directly from the simulations. We also calculated a true contact area A_{Atom} directly from the positions of atoms in the contact. Specifically, the true contact area was calculated as the number of atoms in contact multiplied by the approximate area of an atom.[39] Contact atoms were identified as tip atoms whose time-averaged distance from a substrate atom[50] was less than 0.28 nm, the first peak of the radial distribution function of crystalline Pt, and atom area was approximated as the area of a circle with diameter 0.28 nm.[51]

The ratio between the contact areas calculated from conductance (A_s or A_T) and the *true* contact area obtained from the atom positions (A_{Atom}) is shown in Fig. 5. If there is no oxide, the Sharvin prediction is consistent with that calculated from atom positions. However, as oxide thickness increases, the accuracy of the Sharvin equation decreases, as indicated by the decrease of A_s/A_{atom} from 1 to 0. In contrast, tunneling theory is accurate for the thickest oxides, but underestimates the contact area for thin films, i.e. A_T/A_{atom} increases from 0 to 1 with increasing oxide thickness. Tunneling theory is accurate for the thickest oxides, but underestimates the contact area for thin films, i.e. A_T/A_{atom} increases from 0 to 1 with increasing oxide thickness. Importantly, for oxides between 0.2 and 1.0 nm thick, neither theory appears to be able to provide a reasonable estimate the actual size of the contact. This thickness range is highly relevant to the studies of c-AFM[15] and micro-/nano-electromechanical systems (M/NEMS).[52–54]

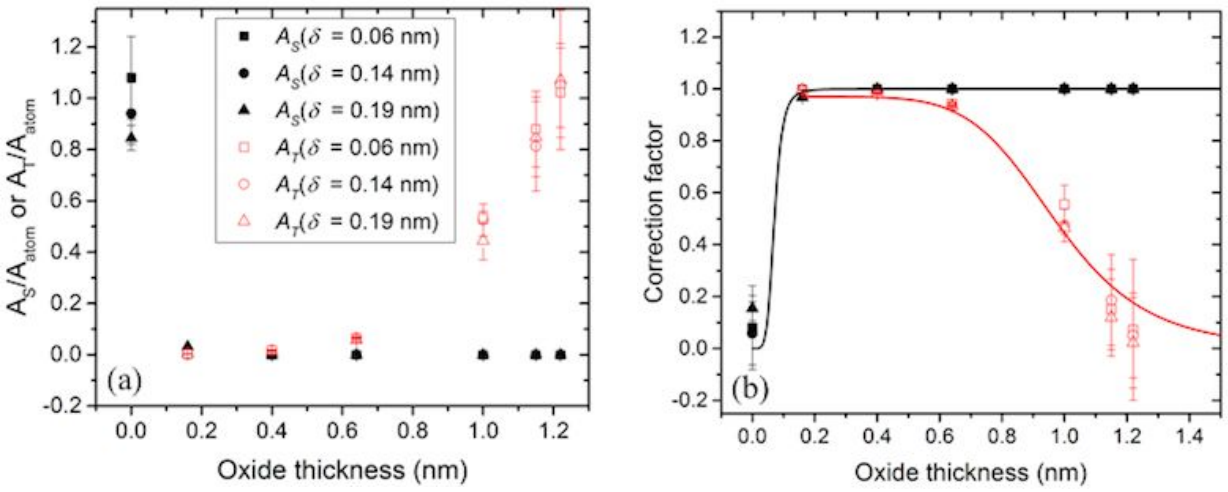

Figure 5: (a) The ratio of contact area calculated from conductance using the Sharvin equation (A_S, black solid symbols) and tunneling theory (A_T, red hollow symbols) to the area calculated from atom positions at different tip-substrate depths (indicated by marker shape). (b) Correction factor for measurement of contact area as a function of oxide thickness, where the symbols have the same meaning as in (a) and the lines correspond to Eqs. 4(a) for ballistic transport (black line) and 4(b) for tunneling (red line).

The difference between true contact area and area calculated from conductance obtained from our simulations is qualitatively consistent with observations from c-AFM experiments. For example, recent experiments using transmission electron microscopy (TEM) of a conductive Pt probe showed that contact area was 95% smaller than predicted by the Sharvin equation and proposed this was due to the presence of a 0.23 nm thick insulating layer, where the thickness was estimated from the resolution of the TEM.[15] Similarly, experimental measurements with a Pt/Ir tip reported that the contact area calculated from conductance was less than 10% of the physical contact area estimated using continuum contact mechanics.[17] This difference was later proposed to be due to insolating surface species not accounted for in the original study.[15] Such findings are consistent with the simulation predictions reported here.

The simulations can be further used to quantify the effect of an oxide on the contact area calculation. The oxide effect was quantified as the normalized difference between the true contact area calculated from atom positions and area calculated from conduction as $c_{S/T} = 1 - \frac{A_{S/T}}{A_{atom}}$. This term represents a correction factor that could be used to calculate true area from a conduction measurement. Figure 5(b) shows the correction factor as a function of oxide thickness. We fitted empirical functions to the contact area data obtained using the Sharvin (c_S) and tunneling (c_T) theories:

$$c_S = 1 - \frac{1}{1 + (\frac{2.10t}{t_0})^{5.42}} \quad (4a)$$

$$c_T = \frac{1}{1 + (\frac{0.15t}{t_0})^{5.17}} \quad (4b)$$

where $t_0 = 0.15\ nm$ is the thickness of a monolayer oxide. The coefficient of determination R^2 is 0.99 for c_S and 0.96 for c_T. For an infinitely thick oxide, these equations predict 100% difference for the Sharvin equation and 0% difference for tunneling theory; in the absence of an oxide, the reverse is true. Further, these functions predict that the accuracy of the conventional theories drops off quickly for oxides with intermediate thickness between 0.2 to 1 nm. For a monolayer oxide ($t = 0.15\ nm$), the deviation from the true contact area is 98% for the Sharvin equation and 99% for tunneling theory.

This study has shown that the Sharvin equation for ballistic transport can be used to calculate contact area from conductance if there is no insulating layer (or a layer assumed to be less than ~0.1 nm thick) and tunneling theory applies for insulating layers thicker than approximately 1 nm. However, for a contact with an insulating layer between these limits, neither theory is expected to provide accurate results. However, in this intermediate range, the functions proposed here can be used to correct results obtained using the Sharvin or tunneling theories. For example, if the thickness of an insulating film is measured or estimated, contact area can be calculated from conductance using tunneling theory and then corrected using Eq. 4(b). Although the correction factors were developed using data for loads up to only tens of nanonewtons, we observe no statistically significant trend in c_S or c_T with load, so anticipate that they will be applicable to higher loading conditions. Therefore, this approach should provide a better measure of contact area than the typical approach of simply assuming ballistic transport using the Sharvin equation.

IV. CONCLUSION

This study investigated the effect of oxide thickness on the contact area that is obtained from conductive AFM. Seven models of platinum tips were created with oxide thicknesses varying from 0 nm (no oxide) to 1.22 nm. The conduction between the tip and the substrate was approximated by identifying atomic channels across the oxide layer, where the conduction through each channel was computed using a DFT-derived current-separation relationship, which accounts for both direct metallic conduction and tunneling conduction. We found that the total conductance dropped rapidly with increasing oxide thickness due to the increasing contribution of tunneling and decreasing contribution of direct metallic conduction. To mimic a c-AFM measurement, the *computed* contact area was obtained from this conductance using a simple application of the Sharvin equation and/or tunneling theory. This computed contact area was compared with the *true* contact area calculated from atom positions at the contacting interface. The difference between the *computed* and *true* values of contact area was analyzed as a function of oxide thickness. The Sharvin equation for ballistic conduction was accurate for the case with no oxide, while tunneling theory provided accurate results for the thickest oxides tested. However, for oxides between 0.2 and 1 nm thick, both theories significantly underpredicted the contact area. This regime of oxide thickness is important for real-world devices because pure platinum typically contains a native surface oxide layer that has been estimated to be less than 0.5 nm thick.[15,21] However, to develop a correction factor for contact area measurements more generally, additional studies will be needed. First, DFT data for conductance through platinum atom channels with oxygen will enable a more accurate empirical model for atom-atom conductance to be developed. Second, simulations of a wider range of tip sizes and loading conditions can capture more possible experimental conditions. Regardless, this work presents a

framework for developing predictive models for contact area. Importantly, the results shown here emphasize that significant error may be associated with estimating contact area in c-AFM using conventional approaches, even for noble metals with only slight (sub-monolayer) coverage of surface layers.

ACKNOWLEDGEMENTS

This work was funded by the National Science Foundation, through award number CMMI-1536800 (University of Pittsburgh) and CMMI-1537613 (University of California Merced).

References

1 J. Y. Park, S. Maier, B. Hendriksen and M. Salmeron, *Mater. Today*, 2010, **13**, 38–45.
2 X. Ou, P. Das Kanungo, R. Kögler, P. Werner, U. Gösele, W. Skorupa and X. Wang, *Nano Lett.*, 2010, **10**, 171–175.
3 H. Hu, H. Kim and S. Somnath, *Micromachines*, 2017, **8**, 90.
4 K. Moth-Poulsen and T. Bjørnholm, *Nat. Nanotechnol.*, 2009, 4, 551–556.
5 O. Y. Loh and H. D. Espinosa, *Nat. Nanotechnol.*, 2012, **7**, 283–295.
6 G. M. Rebeiz and J. B. Muldavin, *IEEE Microw. Mag.*, 2001, **2**, 59–71.
7 T. D. B. Jacobs, T. Junge and L. Pastewka, *Surf. Topogr. Metrol. Prop.*, 2017, **5**, 013001.
8 M. Lantz, S. O'Shea and M. Welland, *Phys. Rev. B - Condens. Matter Mater. Phys.*, 1997, **56**, 15345–15352.
9 M. Enachescu, R. J. a van den Oetelaar, R. W. Carpick, D. F. Ogletree, C. F. J. Flipse and M. Salmeron, *Phys. Rev. Lett.*, 1998, **81**, 1877–1880.
10 A. M. Bratkovsky, A. P. Sutton and T. N. Todorov, *Phys. Rev. B*, 1995, **52**, 5036–5051.
11 N. Agraït, A. L. Yeyati and J. M. van Ruitenbeek, *Phys. Rep.*, 2003, 377, 81–279.
12 L. Olesen, E. Laegsgaard, I. Stensgaard, F. Besenbacher, P. Stoltze and K. W. Jacobsen, *Phys. Rev. Lett.*, 1994, **72**, 2251–2254.
13 L. Chen, H. Lee, Z. J. Guo, N. E. McGruer, K. W. Gilbert, S. Mall, K. D. Leedy and G. G. Adams, *J. Appl. Phys.*, 2007, **102**, 074910.
14 M. Enachescu, R. W. Carpick, D. F. Ogletree and M. Salmeron, *J. Appl. Phys.*, 2004, **95**, 7694–7700.
15 S.B. Vishnubhotla, R. Chen, S. R Khanal, J. Li, E. A. Stach, A. Martini, and T.D.B. Jacobs, *Nanotechnology*, 2019, **30**, 045705.
16 J. G. Simmons, *J. Appl. Phys.*, 1963, **34**, 1793–1803.
17 U. Celano, T. Hantschel, G. Giammaria, R. C. Chintala, T. Conard, H. Bender and W. Vandervorst, *J. Appl. Phys.*, 2015, **117**, 214305.
18 A. Eckmann, A. Felten, A. Mishchenko, L. Britnell, R. Krupke, K. S. Novoselov and C. Casiraghi, *Nano Lett.*, 2012, **12**, 3925–3930.
19 B. P. Brown, L. Picco, M. J. Miles and C. F. J. Faul, *Small*, 2015, **11**, 5054–5058.
20 E. Bussmann, M. Rudolph, G. S. Subramania, S. Misra, S. M. Carr, E. Langlois, J. Dominguez, T. Pluym, M. P. Lilly and M. S. Carroll, *Nanotechnology*, 2015, **26**, 085701.
21 H. Yoshida, H. Omote and S. Takeda, *Nanoscale*, 2014, **6**, 13113–13118.
22 D. Erts, H. Olin, L. Ryen and A. Thölén, *Phys. Rev. B - Condens. Matter Mater. Phys.*, 2000, **61**, 12725–12727.

23 D. J. Oliver, J. Maassen, M. El Ouali, W. Paul, T. Hagedorn, Y. Miyahara, Y. Qi, H. Guo and P. Grutter, *Proc. Natl. Acad. Sci.*, 2012, **109**, 19097–19102.
24 M. Strange, I. S. Kristensen, K. S. Thygesen and K. W. Jacobsen, *J. Chem. Phys.*, 2008, **128**, 114714.
25 S. K. Nielsen, Y. Noat, M. Brandbyge, R. H. M. Smit, K. Hansen, L. Y. Chen, A. I. Yanson, F. Besenbacher and J. M. van Ruitenbeek, *Phys. Rev. B*, 2003, **67**, 245411.
26 V. M. García-Suárez, A. R. Rocha, S. W. Bailey, C. J. Lambert, S. Sanvito and J. Ferrer, *Phys. Rev. Lett.*, 2005, **95**, 256804.
27 M. Strange, K. S. Thygesen and K. W. Jacobsen, *Phys. Rev. B*, 2006, **73**, 125424.
28 L. A. Zotti and R. Pérez, *Phys. Rev. B*, 2017, **95**, 125438.
29 F. Yang, R. W. Carpick and D. J. Srolovitz, *ACS Nano*, 2017, **11**, 490–500.
30 N. Onofrio and A. Strachan, *J. Chem. Phys.*, 2015, **143**, 054109.
31 X. Hu and A. Martini, *Nanoscale*, 2017, **9**, 16852–16857.
32 Y. Jiang, J. A. Harrison, J. David Schall, K. E. Ryan, R. W. Carpick and K. T. Turner, *Tribol. Lett.*, 2017, **65**, 78.
33 Y. Dong, Q. Li and A. Martini, *J. Vac. Sci. Technol. A*, 2013, **31**, 30801.
34 D. Fantauzzi, J. Bandlow, L. Sabo, J. E. Mueller, A. C. T. van Duin and T. Jacob, *Phys. Chem. Chem. Phys.*, 2014, **16**, 23118–23133.
35 D. Fantauzzi, S. Krick Calderón, J. E. Mueller, M. Grabau, C. Papp, H. P. Steinrück, T. P. Senftle, A. C. T. van Duin and T. Jacob, *Angew. Chemie - Int. Ed.*, 2017, **56**, 2594–2598.
36 S. Plimpton, *J. Comput. Phys.*, 1995, **117**, 1–19.
37 L. Maya, L. Riester, T. Thundat and C. S. Yust, *J. Appl. Phys.*, 1998, **84**, 6382–6386.
38 D. Maugis, *J. Colloid Interface Sci.*, 1992, **150**, 243–269.
39 T. D. B. Jacobs and A. Martini, *Appl. Mech. Rev.*, 2017, **69**, 61101.
40 R. H. M. Smit, C. Untiedt, A. I. Yanson and J. M. Van Ruitenbeek, *Phys. Rev. Lett.*, 2001, **87**, 266102-1-266102–4.
41 J. M. Krans, C. J. Muller, I. K. Yanson, T. C. M. Govaert, R. Hesper and J. M. Van Ruitenbeek, *Phys. Rev. B*, 1993, **48**, 14721–14724.
42 J. M. Krans, C. J. Muller, I. K. Yanson and J. M. van Ruitenbeek, *Phys. B Phys. Condens. Matter*, 1994, **194–196**, 1033–1034.
43 R. H. M. Smit, Y. Noat, C. Untiedt, N. D. Lang, M. C. Van Hemert and J. M. Van Ruitenbeek, *Nature*, 2002, **419**, 906–909.
44 M. Strange, K. S. Thygesen, J. P. Sethna and K. W. Jacobsen, *Phys. Rev. Lett.*, 2008, **101**, 096804.
45 W. H. A. Thijssen, M. Strange, J. M. J. aan de Brugh and J. M. van Ruitenbeek, *New J. Phys.*, 2008, **10**, 033005.
46 V. M. García-Suárez, A. R. Rocha, S. W. Bailey, C. J. Lambert, S. Sanvito and J. Ferrer, *Phys. Rev. B*, 2005, **72**, 045437.
47 K. S. Thygesen and K. W. Jacobsen, *Phys. Rev. Lett.*, 2005, **94**, 036807.
48 J. M. Krans and J. M. Van Ruitenbeek, *Phys. Rev. B*, 1994, **50**, 17659–17661.
49 J. Bao and D. D. Macdonald, *ECS Trans.*, 2007, **3**, 1–13.
50 S. Cheng and M. O. Robbins, *Tribol. Lett.*, 2010, **39**, 329–348.
51 S. Solhjoo and A. I. Vakis, *Comput. Mater. Sci.*, 2015, **109**, 172–182.
52 R. A. Coutu, P. E. Kladitis, K. D. Leedy and R. L. Crane, *J. Micromechanics Microengineering*, 2004, **14**, 1157–1164.
53 H. Lee, R. A. Coutu, S. Mall and K. D. Leedy, *J. Micromechanics Microengineering*,

2006, **16**, 557–563.
54 L. Chen, H. Lee, Z. J. Guo, N. E. McGruer, K. W. Gilbert, S. Mall, K. D. Leedy and G. G. Adams, *J. Appl. Phys.*, 2007, **102**, 074910.

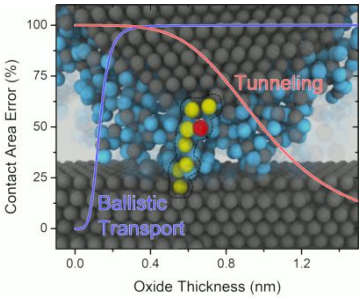

Simulations provide a way to calculate contact area from conductive atomic force microscopy measurements of platinum with a thin insulating layer.